X-811-71-392
PREPRINT

THE CALCULATION OF ELECTROMAGNETIC FIELDS IN THE FRESNEL AND FRAUNHOFER REGIONS USING NUMERICAL INTEGRATION METHODS

RICHARD F. SCHMIDT

JULY 1971

GSFC
GODDARD SPACE FLIGHT CENTER
GREENBELT, MARYLAND

X-811-71-392

THE CALCULATION OF ELECTROMAGNETIC FIELDS IN THE FRESNEL AND FRAUNHOFER REGIONS USING NUMERICAL INTEGRATION METHODS

Richard F. Schmidt

July 1971

Goddard Space Flight Center
Greenbelt, Maryland

THE CALCULATION OF ELECTROMAGNETIC FIELDS IN THE FRESNEL AND FRAUNHOFER REGIONS USING NUMERICAL INTEGRATION METHODS

Richard F. Schmidt
Network Engineering Division

ABSTRACT

This document presents some results obtained with a digital computer program written at Goddard Space Flight Center to obtain electromagnetic fields scattered by perfectly reflecting surfaces. For purposes of illustration a paraboloidal reflector is illuminated at radio frequencies in the simulation for both receiving and transmitting modes of operation. Fields are computed in the Fresnel and Fraunhofer regions. A dual-reflector system (Cassegrain) is also simulated for the transmitting case, and fields are computed in the Fraunhofer region.

Appended results include derivations which show that the vector Kirchhoff-Kottler formulation has an equivalent form requiring only incident magnetic fields as a driving function. Satisfaction of the radiation conditions at infinity by the equivalent form is demonstrated by a conversion from Cartesian to spherical vector operators. A subsequent development presents the formulation by which Fresnel or Fraunhofer patterns are obtainable for dual-reflector systems. A discussion of the time-average Poynting vector is also appended.

CONTENTS

ILLUSTRATIONS

ILLUSTRATIONS (Continued)

GLOSSARY OF NOTATION

Symbol	Meaning
$\bar{E}(x', y', z')\bar{H}(x', y', z')$	backscattered electric and magnetic fields at observer position (x', y',z')
μ, ϵ, σ	constitutive parameters: magnetic permeability, inductive capacity, electric conductivity
ω	angular frequency
j, i	imaginary operator = $\sqrt{-1}$
$\bar{E}_1$, $\bar{H}_1$; $\bar{E}_2$, $\bar{H}_2$	electric and magnetic illumination distribution fields
ψ	solution to the wave equation
$\nabla\psi$	vector gradient of ψ
d s	differential area
d ℓ	differential arc-length
$\bar{n}$	unit normal to a surface
$\bar{e}_i$, $\bar{h}_i$	electric and magnetic polarization vectors
$\bar{\rho}$	vector from a feed point to a surface
$\bar{v}$	a vector used to generate $\bar{e}_i$ and $\bar{h}_i$ for a spherical wave
O	order, origin
k	wave number = $2\pi/\lambda$
λ	wavelength
r	radial distance in spherical system
θ	polar angle in spherical system
ϕ	azimuthal angle in spherical system
$\hat{1}_r$, $\hat{1}_\theta$, $\hat{1}_\phi$	unit vectors in spherical system
D	aperture diameter
$\langle\bar{P}\rangle$	time-average Poynting vector
R	distance from origin O
F	focal length of a paraboloid

Δ feed displacement in focal-plane

K beam deviation factor

θ_s beam squint angle

$\bar{K}$ electric sheet current

q_s, q_ℓ electric surface and line charges

σ, ζ radial and angular variables for surfaces in parametric form

THE CALCULATION OF ELECTROMAGNETIC FIELDS IN THE FRESNEL AND FRAUNHOFER REGIONS USING NUMERICAL INTEGRATION METHODS

INTRODUCTION

The purpose of this document is (1) to present some computed results obtained with the Kirchhoff-Kottler formulation in the Fresnel and Fraunhofer regions, (2) to discuss equivalent scattering formulations, (3) to introduce a simplification in the procedure for obtaining Fresnel and Fraunhofer patterns for dual-reflector systems, and (4) to derive the expression used for the time-average Poynting vector in the digital computer program.

The results obtained here are based on the contributions of many persons. It is impossible to acknowledge all of them properly. Most of the fundamental ideas were well-developed many years ago, but the advent of the fast digital computer has, within the past 5 years, made possible the numerical evaluation of existing formulations for practical geometries, feeds etc. Since this document contains representative results in Fresnel as well as Fraunhofer regions, some of the language and concepts of optics are introduced. The bright diffraction disc and rings of Airy, for example, are especially significant in the reception mode of operation (image space). A brief historical outline is included. Most of the dates and comments in this introduction were taken from textbooks, journal articles, etc.

History of Diffraction

1452-1519	da Vinci:	first reference to diffraction
1601-1665	Fermat:	principle of least time which implied rectilinear propagation, independent rays, law of reflection, law of refraction
1621	Snell:	sometimes credited with laws of reflection and refraction
1663	Gregory:	"Gregorian" dual-reflector system
1663	Cassegrain:	"Cassegrainian" dual-reflector system
1665	Grimaldi:	first accurate descriptions of diffraction
1690	Huygens:	first proponent of wave theory without periodicity

1642-1727	Newton:	corpuscular theory (received acceptance for 100 years) to the exclusion of Huygens wave theory
1718	Maraldi:	found the "Arago" spot in the umbral region
1817	Young:	suggested transverse rather than longitudinal wave motion and the interference principle
1818-1827	Fresnel:	extended Huygens' theory by adding periodicity in time and space to the wavefronts, but several arguments had no physical significance. Accounted for rectilinear propagation as $\lambda \to 0$, reflection, refraction, and diffraction effects. Predicted bright spot in disc umbra
1818	Poisson:	reviewed Fresnel's prize memoir, and refuted conclusion of bright spot in shadow of disc
1818	Arago:	verified Fresnel's bright spot by experiment
1827	Fraunhofer:	diffraction formulations, measurements
1824-1844	Hamilton:	geometrical optics (ignored Huygens' and Newton's formulation; indifferent to physical interpretation and interference concepts)
1834	Airy:	calculation of diffraction disc and rings
1849	Stokes:	limited version of general treatment later made by Kirchhoff
1865	Maxwell:	wrote the fundamental equations of electromagnetic theory $\nabla \times \bar{E} = -\partial \bar{B}/\partial t$ and $\nabla \times \bar{H} = \bar{J} + \partial \bar{D}/\partial t$
1882	Kirchhoff:	wrote the Kirchhoff-Helmholtz Integral Theorem, $$\psi(x', y', z') = \frac{1}{4\pi} \int_s \left[\psi \frac{\partial}{\partial n}\left(\frac{e^{ikr}}{r}\right) - \frac{e^{ikr}}{r} \frac{\partial \psi}{\partial n} \right] d s.$$ Kirchhoff started with the scaler wave equation in three dimensions, and deduced a formulation which in many respects embodies the basic ideas of the Huygens-Fresnel principle.
1883	Poynting:	theorem on energy flow
1888	Maggi:	provided additional insight on Kirchhoff theory, including a transformation for an unclosed surface with rim Γ.

1893	Heaviside:	studied the energy flow problem and physical interpretation of formulations
1909	Debye:	analytical work on scattering
1909	Reiche:	investigated axial non-linear phase shift
1911	Sommerfeld:	rigorous analytical solutions, used boundary value approach
1917	Rubinowicz:	preceded Kottler in studies of unclosed surfaces with rim
1923	Kottler:	showed that Kirchhoff's solution to the black-screen diffraction problem was a first approximation to a boundary value problem (actually a solution to a "saltus" problem). Kottler annexed a contour integral, for unclosed surfaces, to the Kirchoff formulation.
1939	Stratton and Chu:	further analysis of Kottler's contour integral and its relationship to Maxwell's equations
1957	Keller:	presented an extension of the theory of geometrical optics
1967	Sancer:	showed that the vector Kirchhoff equations can be derived using the free-space dyadic Green's function and the appropriate Green's theorem. The Kottler contour integral was obtained without appeal to physical intuition, and was inherently contained in the derivation rather than appended at the close (the historical development.

The preceding partial list of contributors is indicative of the broad field of analysis and research associated with the subject of diffraction. In this document the Kirchhoff-Kottler formulation has been stressed with a view toward obtaining meaningful solutions for practical feed-reflector configurations. Exploration of the bounds of validity of the selected theory is predicated on objective comparisons with other analyses and direct physical measurements where practicable. The interested reader may wish to review the mathematical and physical reasoning which underlie the Kirchhoff-Kottler theory of diffraction. Problems associated with the definition of a black screen, the introduction of polarization in a physical 3-space, and finite surfaces are discussed in detail in numerous textbooks [1] and will not be considered here. The extrapolation from the original

[1] Ref. 1, Chapter II.
Ref. 2, pp. 460-470
Ref. 3, Chapter 5
Ref. 4, Chapter VIII

black-screen derivations to present day applications, such as those involving multimode waveguide feeds in dual-reflector systems, provides a sharp contrast. A review of the analytic difficulties encountered in the theory, the departure from the assumption of continuity required by the underlying Green's theorem, and the additional compromises due to numerical evaluation should be weighed against nearly a century of useful predictions resulting from the Kirchhoff theory. Barakat[1], in paraphrasing a remark of Poincaré, said "The theoreticians believe in the Kirchhoff theory because they hold it to be an experimental fact, while the experimentalists think it to be a mathematical theorem." The statement is a tribute to the theory considering that scatterer size, observer range, and radii of curvature of both scatterer and wavefront must be large in terms of a wavelength. Further, the effect of mutual coupling on the scatterer, and between source and scatterer, are traditionally neglected altogether.

FORMULATION OF THE SCATTERED FIELDS

The formulation for the scattered electric and magnetic fields from perfectly conducting surfaces is taken as [2]

$$\bar{E}(x', y', z') = \frac{1}{j\omega\epsilon}\frac{1}{4\pi}\int_{S_1}[(\bar{n}\times\bar{H}_1)\cdot\nabla]\nabla\psi\, ds - j\omega\mu\frac{1}{4\pi}\int_{S_1}(\bar{n}\times\bar{H}_1)\psi\, ds$$

$$\bar{H}(x', y', z') = -\frac{1}{4\pi}\int_{S_1}(\bar{n}\times\bar{H}_1)\times\nabla\psi\, ds,$$

where

$$\psi = \frac{e^{-ikr}}{r}, \quad \nabla\psi = -\left(jk + \frac{1}{r}\right)\psi\,\hat{1}_r$$

Previously, the equivalent electric-field formulation

$$\bar{E}(x', y', z') = -\frac{1}{j\omega\epsilon}\frac{1}{4\pi}\int_c \nabla\psi\,\bar{H}_1\cdot d\bar{\ell} - \frac{1}{4\pi}\int_{S_1}[j\omega\mu(\bar{n}\times\bar{H}_1)\psi + (\bar{n}\cdot\bar{E}_1)\nabla\psi]\, ds$$

[1] Ref. 5 Chapter 9, pp. 6-16

[2] Appendix A provides background for this formulation from several sources.

was employed.[1] The latter formulation for $\overline{E}(x',y',z')$ could be termed the "historical" approach since the Kottler contour integral appears explicitly as an amendment to the Kirchhoff formulation. It has been shown that this line-charge integral can be obtained along with the Kirchhoff formulation without appeal to physical intuition via a dyadic Green's function,[2] and further, the two forms for $E(x',y',z')$ yield identical results.

From a programmer's viewpoint the organization of the problem is complicated by the "historical" formulation for the electric field $\overline{E}(x',y',z')$. It is noted that a mixture of contour and surface integrals requires separate quantizing or sampling intervals for numerical evaluation. In addition, the surface-charge integral appearing in the "historical" formulation involves the incident electric field, so that the polarization vector $\overline{e}_i$ must also be developed and retained in the numerical evaluation. This should be contrasted with the formulation used herein, which proceeds simply with surface integrals, the incident magnetic field, and the associated magnetic polarization vector $\overline{h}_i$ for the incident wave.

$$\overline{e}_i = \frac{\overline{\rho}_1 \times (\overline{v} \times \overline{\rho}_1)}{|\overline{\rho}_1 \times (\overline{v} \times \overline{\rho}_1)|}$$

$$\overline{h}_i = \frac{\overline{\rho}_1 \times \overline{v}}{|\overline{\rho}_1 \times v|}$$

Unless there is a specific reason for distinguishing the Kottler line-charge integral and Kirchhoff surface-charge integral contributions in a problem, their combined influence can be computed via the surface integral

$$\frac{1}{j\,\omega\,\epsilon}\,\frac{1}{4\pi}\int_{s_1}\left[(\overline{n}\times\overline{H}_1)\cdot\nabla\right]\nabla\psi\,ds$$

for the total bound electric charge distribution. It is easy to verify that the formulation for $\overline{E}(x',y',z')$ and $\overline{H}(x',y',z')$ satisfy the radiation condition at infinity. A slight complication is encountered with the operator del, written

$$\nabla = \hat{i}\,\frac{\partial}{\partial x} + \hat{j}\,\frac{\partial}{\partial y} + \hat{k}\,\frac{\partial}{\partial z}$$

in Cartesian coordinates.

[1] Ref. 2, page 469

[2] Ref. 6

The radial component, at infinity, of the integral

$$-j\omega\mu\frac{1}{4\pi}\int_{S_1}(\bar{n}\times\bar{H}_1)\,\psi\,ds$$

can be set down immediately as

$$-j\,\omega\mu\frac{1}{4\,\omega\mu}\int_{S_1}[(\bar{n}\times\bar{H}_1)\,\psi\cdot\hat{1}_r]\,\hat{1}_r\,ds$$

The integral

$$\frac{1}{j\,\omega\epsilon}\frac{1}{4\pi}\int_{S_1}[(\bar{n}\times\bar{H}_1)\cdot\nabla]\,\nabla\psi\,ds$$

is entirely radial at infinity, as is anticipated for charges, however, manipulation of the integrand in terms of the Cartesian operator ∇ is undesirable since

$$\nabla\psi=-\left(j\,k+\frac{1}{k}\right)\psi\,\hat{1}_k$$

is radial.[1] An interpretation of $(\bar{n}\times\bar{H}_1)\cdot\nabla$ in spherical coordinates is, therefore, needed to establish the vanishing of the radial part of the electric field at infinity.

A vector dot product in orthogonal curvilinear coordinates can be defined as[2]

$$\bar{p}\cdot\bar{q}=p_u\,q_u+p_v\,q_v+p_w\,q_w$$

and the dot product $(\bar{n}\times\bar{H}_1)\cdot\nabla$ should follow directly except for the fact that $\bar{p}\rightarrow(\bar{n}\times\bar{H}_1)$ is a vector, and $\bar{q}\rightarrow\nabla$ is an operator. Furthermore, the form of ∇ in spherical coordinates depends on the operation to be performed, which is unlike the Cartesian case where ∇ is the same for grad, div, curl, cross-product, and dot-product.

---

[1] The numerical evaluation of $[(\bar{n}\times\bar{H}_1)\cdot\nabla]\cdot\nabla\psi$ also needs to be considered. A conversion of $\nabla\psi$ from spherical to Cartesian coordinates was used previously in the program, posing no problems, but in the present formulation

$$(\bar{n}\times\bar{H}_1)\cdot\nabla=K_x\frac{\partial}{\partial x}+K_y\frac{\partial}{\partial y}+K_z\frac{\partial}{\partial z}$$

is a differential operator, and $\nabla\psi$ is a numerical result for each differential area ds.

[2] Ref. 7, page 155.

The form of ∇ to be used is suggested by the quantity on which scalar form $[(\bar{n} \times \bar{H}_1) \cdot \nabla]$ operates. Here

$$\nabla \psi = - \left(j\, k + \frac{1}{r} \right) \psi\, \hat{1}_r$$

is a function of (r) alone, and is a vector. The spherical basis vector $\hat{1}_r$ is invariant with radial changes. From orthogonal curvilinear coordinate relationships,[1] the gradient of a scalar (ξ) in spherical coordinate is

$$\nabla \xi = \frac{1}{\alpha} \frac{\partial \xi}{\partial r} \hat{1}_r + \frac{1}{\beta} \frac{\partial \xi}{\partial \theta} \hat{1}_\theta + \frac{1}{\gamma} \frac{\partial \xi}{\partial \phi} \hat{1}_\phi,$$

and

$$\alpha = \left| \frac{\partial}{\partial r} (r\, \hat{1}_r) \right| = 1$$

$$\beta = \left| \frac{\partial}{\partial \theta} (r\, \hat{1}_r) \right| = r$$

$$\gamma = \left| \frac{\partial}{\partial \phi} (r\, \hat{1}_r) \right| = r \sin \theta.$$

Then

$$[(\bar{n} \times \bar{H}_1) \cdot \nabla] \cdot \nabla \psi = \left[(\bar{n} \times \bar{H}_1) \cdot \hat{1}_r \frac{\partial}{\partial r} \right] \nabla \psi = [(n \times \bar{H}_1) \cdot \hat{1}_r] \frac{\partial^2 \psi}{\partial r^2} \hat{1}_r$$

$$= \hat{1}_r \left(- k^2 + 2 \frac{j\, k}{r} + \frac{2}{r^2} \right) \psi\, [(\bar{n} \times \bar{H}_1) \cdot \hat{1}_r]$$

which shows (1/r) in orders O^1, O^2, O^3 since $\psi = e^{-jkr}/r$. The highest order of the term (1/r) in the formulation for $\bar{E}(x',y',z')$ containing the contour integral is O^2.

[1] Ref. 7, page 152

Vanishing the radial fields at infinity is now made very simple.[1] Summing the radial parts of

$$\bar{E}(x', y', z') = \frac{1}{j\omega\epsilon}\frac{1}{4\pi}\int_{S_1}[(\bar{n}\times\bar{H}_1)\cdot\nabla]\,\nabla\psi\,ds - j\omega\mu\frac{1}{4\pi}\int_{S_1}(\bar{n}\times\bar{H}_1)\,\psi\,ds$$

at infinity, terms of O^2, O^3 in $(1/r)$ are neglected. Remaining terms of O^1 in $(1/r)$ annihilate.

$$\frac{1}{4\pi}\left[\left(\frac{-k^2\psi}{j\omega\epsilon} - j\omega\mu\psi\right)(\bar{n}\times\bar{H}_1)\cdot\hat{1}_r\right]\hat{1}_r = 0$$

and

$$c = f\lambda = \frac{1}{\sqrt{\mu\epsilon}},$$

an identity, is recovered.

The magnetic field is inherently simpler due to the absence of bound magnetic charges.

$$\bar{H}(x', y', z') = -\frac{1}{4\pi}\int_{S_1}(\bar{n}\times\bar{H}_1)\times\nabla\psi\,ds.$$

This field is transverse since $\nabla\psi$ is radial at infinity and the cross-product of two vectors is orthogonal to the vectors entering into that cross-product.

---

[1] The numerical evaluation can also be carried out now since the integrand $[(n\times\bar{H}_1)\cdot\nabla]\,\nabla\psi$ has been rewritten as $\hat{1}_r(-k^2 + 2jk/r + 2/r^2)\psi$ which is convertibile to Cartesian components and free of troublesome operators. $\nabla\psi = -(jk + 1/r)\psi\hat{1}_r$ is assumed to be reduced to the Cartesian or "working notation" of the program already.

Figure 1. NASA Tracking Station, Rosman, N.C.

SINGLE-REFLECTOR SYSTEMS

The vector Kirchhoff-Kottler diffraction theory is applied here to the study of paraboloidal systems, initially, then to the conics, and subsequently to distorted conics and more general surfaces exhibiting aberrations of various kinds. Results presented in this document are principally for the paraboloid in both transmit and receive modes of operation.[1] The paraboloid is singular in its focussing properties, has found wide application in optics and microwave technology, and extensive data exists for it in the literature. Particularly interesting are those paraboloids with small f numbers ($f = F/D < 0.5$) as these are encountered often in radio-frequency applications and are somewhat more difficult to analyze [2] than the large F/D structures.

A typical RAD HAZ environment exists in the installation at the NASA tracking station (Rosman, N. C.) shown in Fig. 1. Some years ago (circa 1964) a study of the possible radiation hazard existing on one of the access roads was undertaken. The only methods available at that time were awkard and empirical.[3] In general, the field-strength and energy-density levels at a set of points in the vicinity of a high-gain paraboloid energized by a high-power transmitter were sought. Without trying to re-create the precise set of conditions at Rosman, an attempt will be made to illustrate how the Diffraction Program developed at Goddard Space Flight Center might be used, not only in a RAD-HAZ application, but also in a more general way to design feeds for scanned beams, explore other reflector geometries, and capture energy from the Airy-type diffractions rings, etc.

To illustrate the RAD-HAZ application: Fig. 2 and Fig. 3 show the transmitted electric field versus angle θ as the radius of the observer is reduced from 100 miles through $2D^2/\lambda$, $1D^2/\lambda$, and $D^2/2\lambda$. Coordinates in the field explored by these four arcs are representative of the access road mentioned previously. The object is to determine amplitude, and to a lesser degree polarization and phase in a RAD-HAZ study. It can be seen that the field pattern shape is only slightly degraded in the Fraunhofer region between 100 miles and $2D^2/\lambda$.

---

[1] The results presented in this document formed the basis of a presentation give at the 1971 USNC-URSI Spring Meeting, Washington, D. C. under Commission I, Near-Field Measurements and Radiation Hazards Probing (RAD HAZ).

[2] Ref. 11, page 485
Ref. 12, page 353

[3] Ref. 13, see section on antennas (power density multiplication)

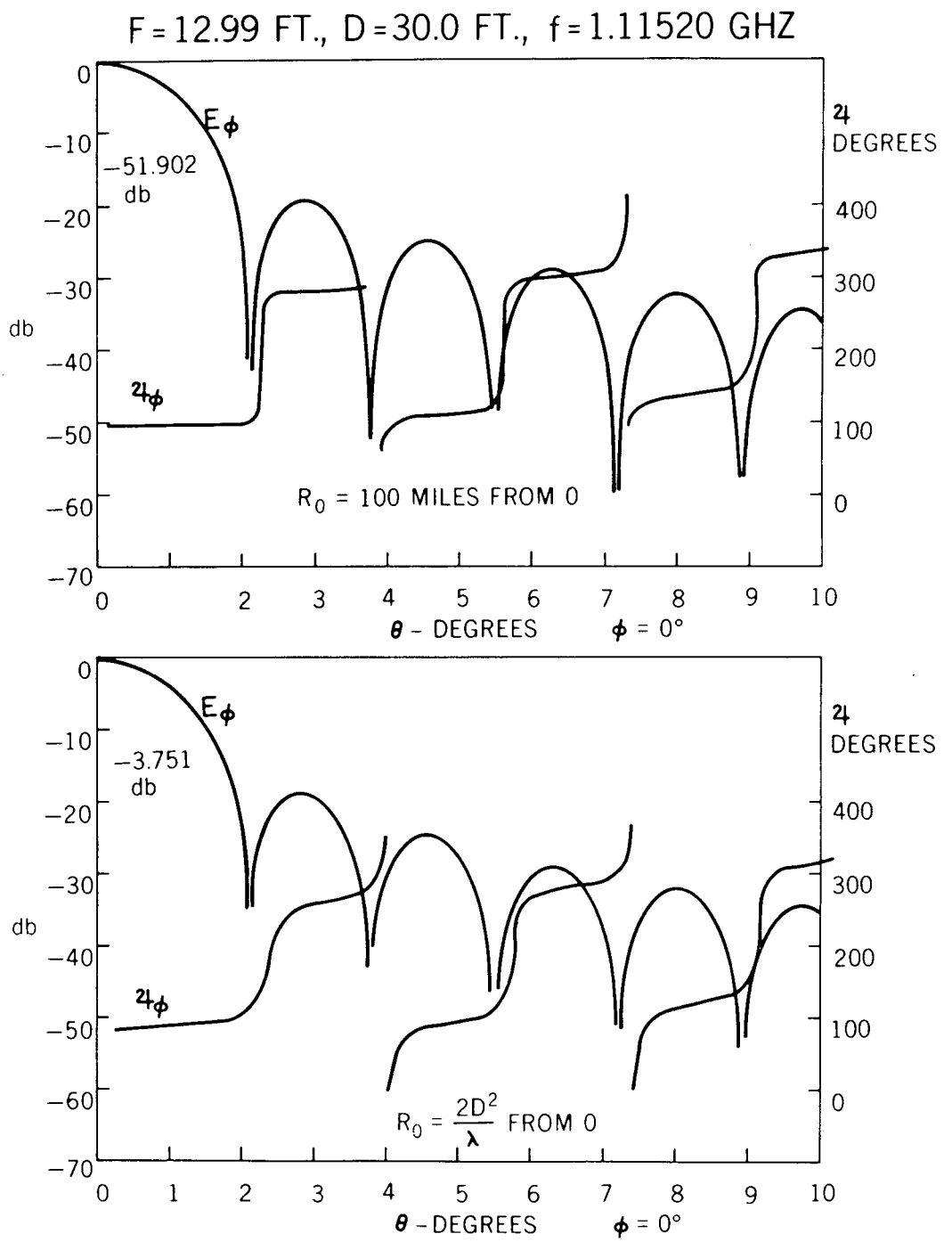

Figure 2. Electric Field vs. Angle θ

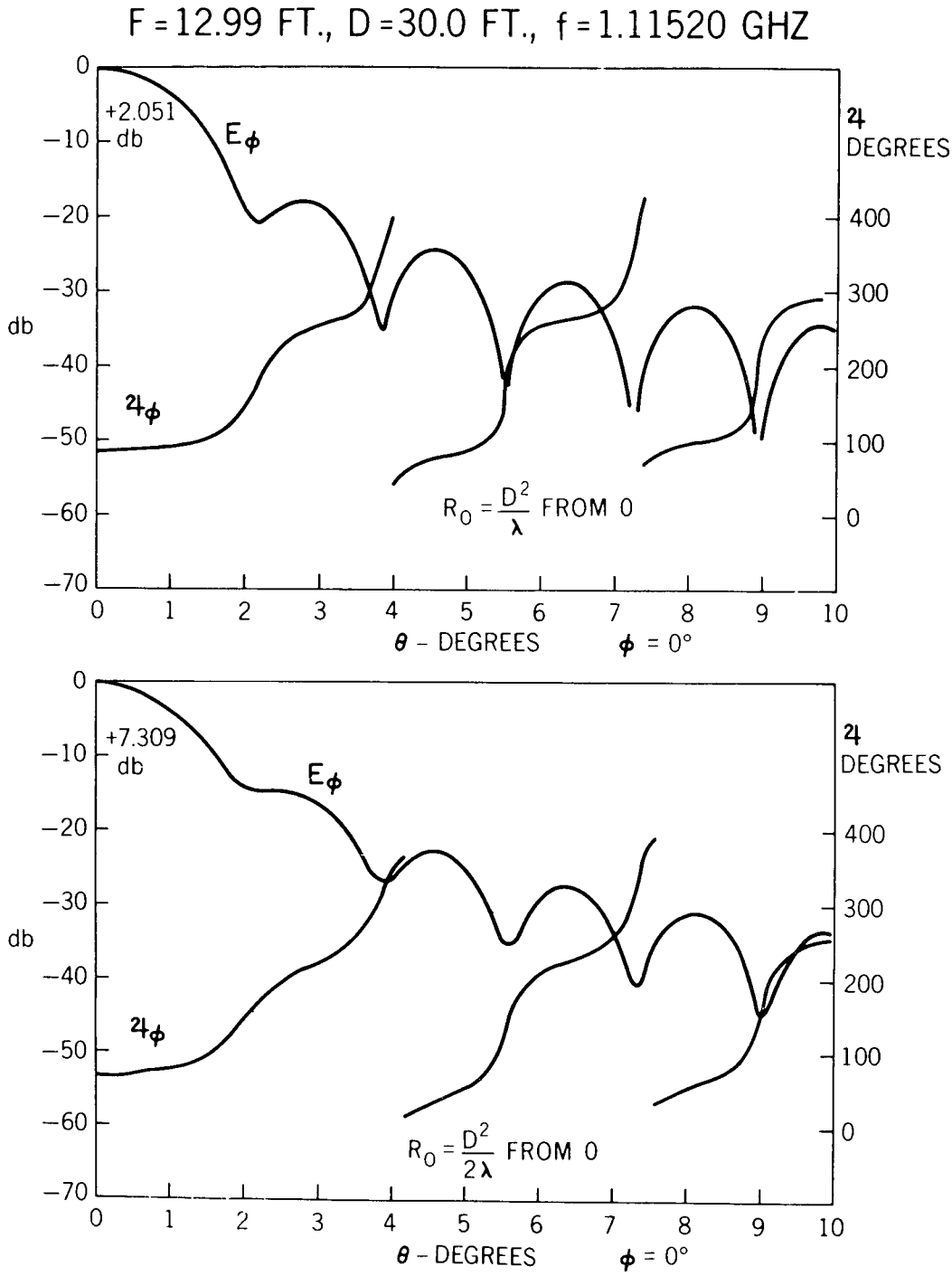

Figure 3. Electric Field vs. Angle θ

Some null-filling is in evidence, the π-radian phase jumps at pattern nulls have become more gradual transitions at pattern minima and signal level is nearly proportional to 1/R. Within the $2D^2/\lambda$ arc the pattern is unique for each radius, null-filling is pronounced, beamwidth is increased, and the signal level no longer varies as the inverse first-power of distance.

As the paraboloid is approached more closely, the moving spherical triad of basis vectors conforms poorly to the transmitted wave which, in the focal plane (R = 0), resembles a plane wave more than a spherical wave. For this reason the Cartesian basis is used to resolve the fields. In addition, the time-averaged Poynting vector is now displayed.[1] See Fig. 4. The region considered is centered about the axial point $D^2/2\lambda$ from the focus of the paraboloid. To the far-left of the area shown by Fig. 4, the more intense time-average Poynting vectors $< \overline{P} >$ form a nearly parallel bundle whose diameter is roughly that of the paraboloid. To the far-right of the area shown, the vectors $< \overline{P} >$ diverge and appear to come from origin O, which is also the focal-point F of the paraboloid. That is, the set of vectors $< \overline{P} >$ in the Fraunhofer region appear to flow radially from a point origin, but their intensity is modulated in accordance with the envelope shown by Fig. 2. Fig. 4 is interesting because it shows that transition region where the Poynting vectors $< \overline{P} >$ have not quite aligned themselves with the lines tracing back to origin O. No attempt was made to scale the length of the power flow vectors $< \overline{P} >$, but it was noted that those vectors which departed considerably from the lines intersecting at O were also reduced in intensity.

A measured result, obtained for a region between the focal point and a point approximately 17λ further away from the transmitting paraboloid, is shown in the text by Collin and Zucker.[2] It is noted that although the discussion has been limited to paraboloids with focal-point excitation, the program is written in a general way to accept other surfaces, including distorted conics, etc. and there is no restriction on the number of feeds, method of excitation, position of feeds etc., other than those restrictions inherently imposed by the Kirchhoff theory itself.

At this point it is convenient to invoke reciprocity and study some of the fields obtained from reflectors in the receiving mode of operation. The received fields are less intense than the transmitted fields, above, and do not constitute a RAD-HAZ problem in the preceding context, however, an element of RAD-HAZ is still present since, for the case of paraboloids, spheres and other reflectors, energy is being concentrated in a relatively small region. From a standpoint of feed design, the received fields provide a means of matching feeds to fields (frequently in a conjugate sense). The literature of optics abounds in both experimental and theoretical studies of the image space.[3] As before, the paraboloid

[1] Appendix B
[2] Ref. 14, page 50
[3] Ref. 4, pp. 435-480

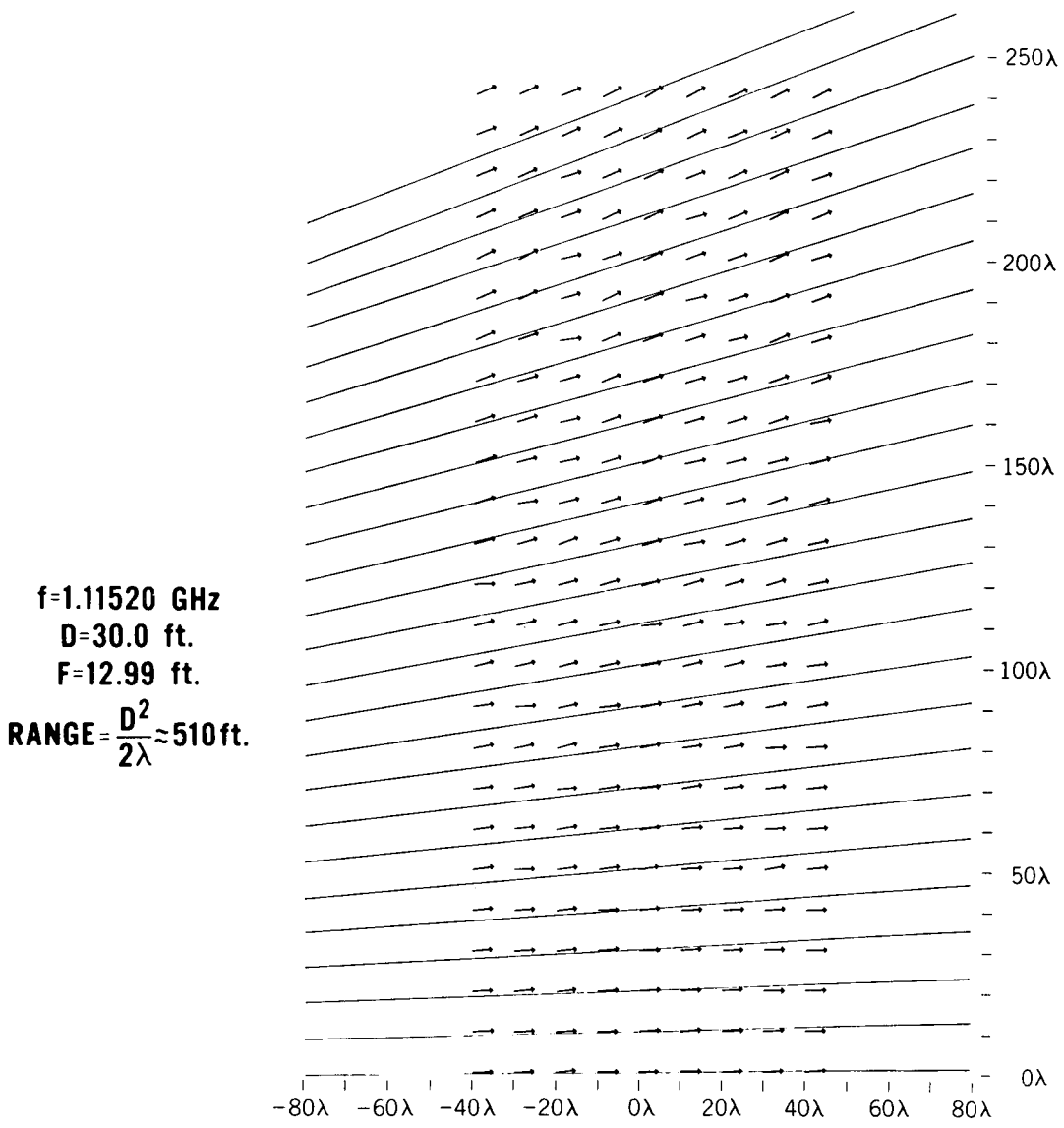

Figure 4. Direction of the time-average Pointing vector

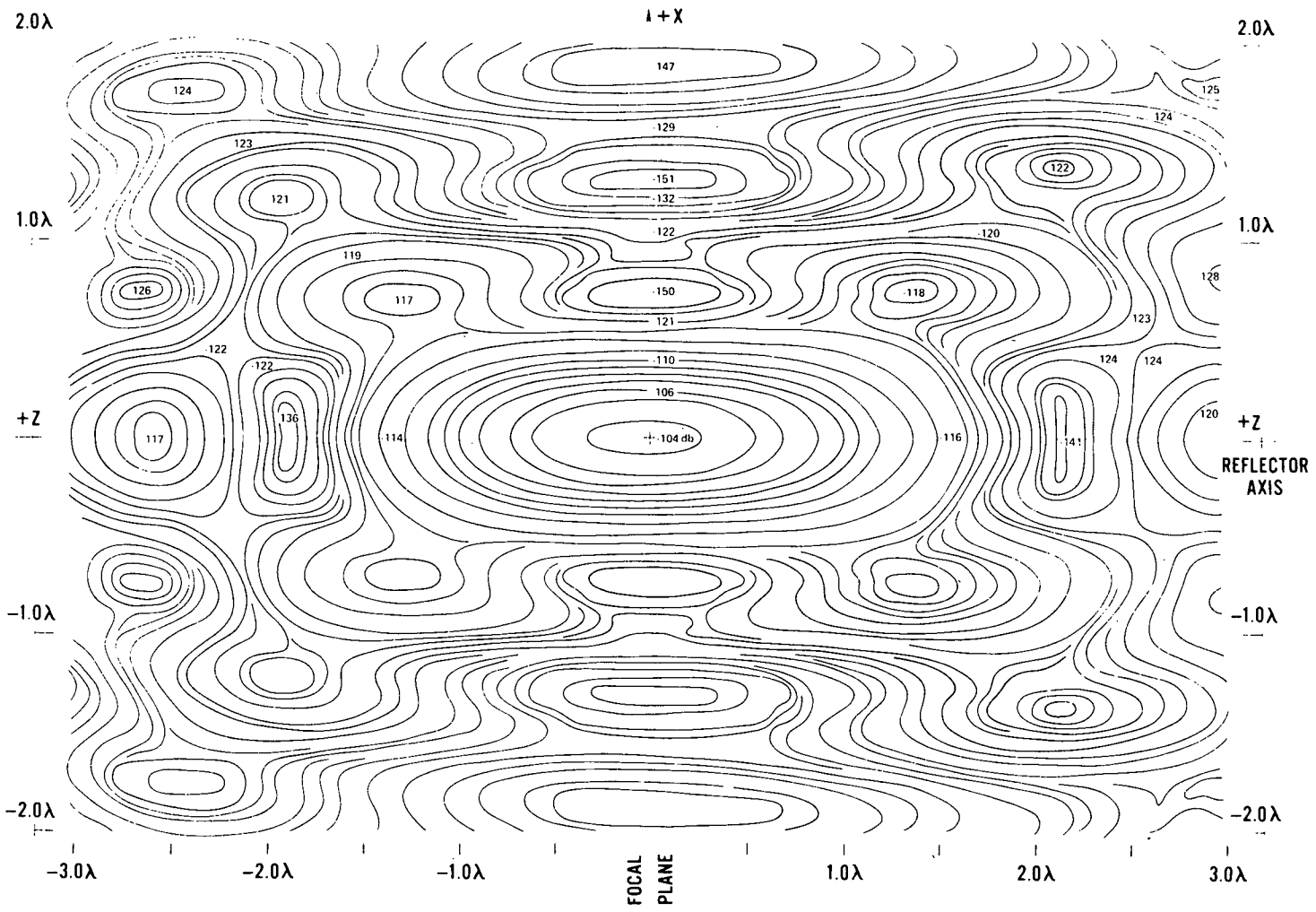

Figure 5. Amplitude of magnetic field near focal-plane (axial reception)

is utilized here for convenience and because its properties are well-known. An objective of the program, however, is to obtain insight for those scattering systems that are difficult to treat analytically and for which only meager data can be found in the literature.

The constant field intensity plots (isophotes) shown in Fig. 5 are for the focal-region of an ideal paraboloid for the axial reception of a plane-wave. The source in this case is to the right, the scatterer to the left, and the converging spherical wave is progressing from left to right. This convention will be retained in all of the subsequent examples. Results are symmetrical about the y-z plane, but asymmetrical about the focal plane. The F/D of this system is only 0.433, therefore, energy flows into the image space at a steep angle. Fig. 6 shows the Airy disc and rings in the x-y on focal plane.

The phase of the electric field is shown in Fig. 7 for the preceding set of isophotes (Fig. 5) over a restricted portion of the z-axis ($\pm 1\lambda$ re O). Power-flow in this region is orthogonal to these wave fronts. It is also apparent that there is no rational definition of phase for axial nulls, and zero-intensity rings of the Airy pattern. Energy flow is around such singular points.

A plot of the direction of the time-average Poynting vector $<\bar{P}>$ for the focal region being discussed is given as Fig. 8. The crossed lines are the bounds of the geometrical shadow. Airy discs, bright rings, and dark rings can be seen without difficulty. No attempt was made here to scale the length of vector $<\bar{P}>$ in accordance with its magnitude, however, this capability has now been automated in a Calcomp plot program. The turbulent regions to the left and right of the geometrical focus correspond to the limits of the depth of field at which the intensity of field vanishes. It is noted that the time-average Poynting vectors do not cross the system axis, which is distinct from a ray-optics presentation, but rather diverge as if they originated from F for large z.

Especially interesting is the region surrounding a null. The null between the Airy bright disc and the first bright ring is shown in Fig. 9. A circulation or vortex-like flow can be seen about the null and an examination of the magnitude of $<\bar{P}>$ shows that the intensity of the time-average Poynting vector diminishes in a continuous manner as the null in the vortex is approached. The existence of this counter-flow of energy has been reported previously, and was computed by Minnett and Thomas[1] who used axial-wave theory to investigate the characteristics of fields in the focal region of a paraboloidal reflector.

[1] Ref. 15

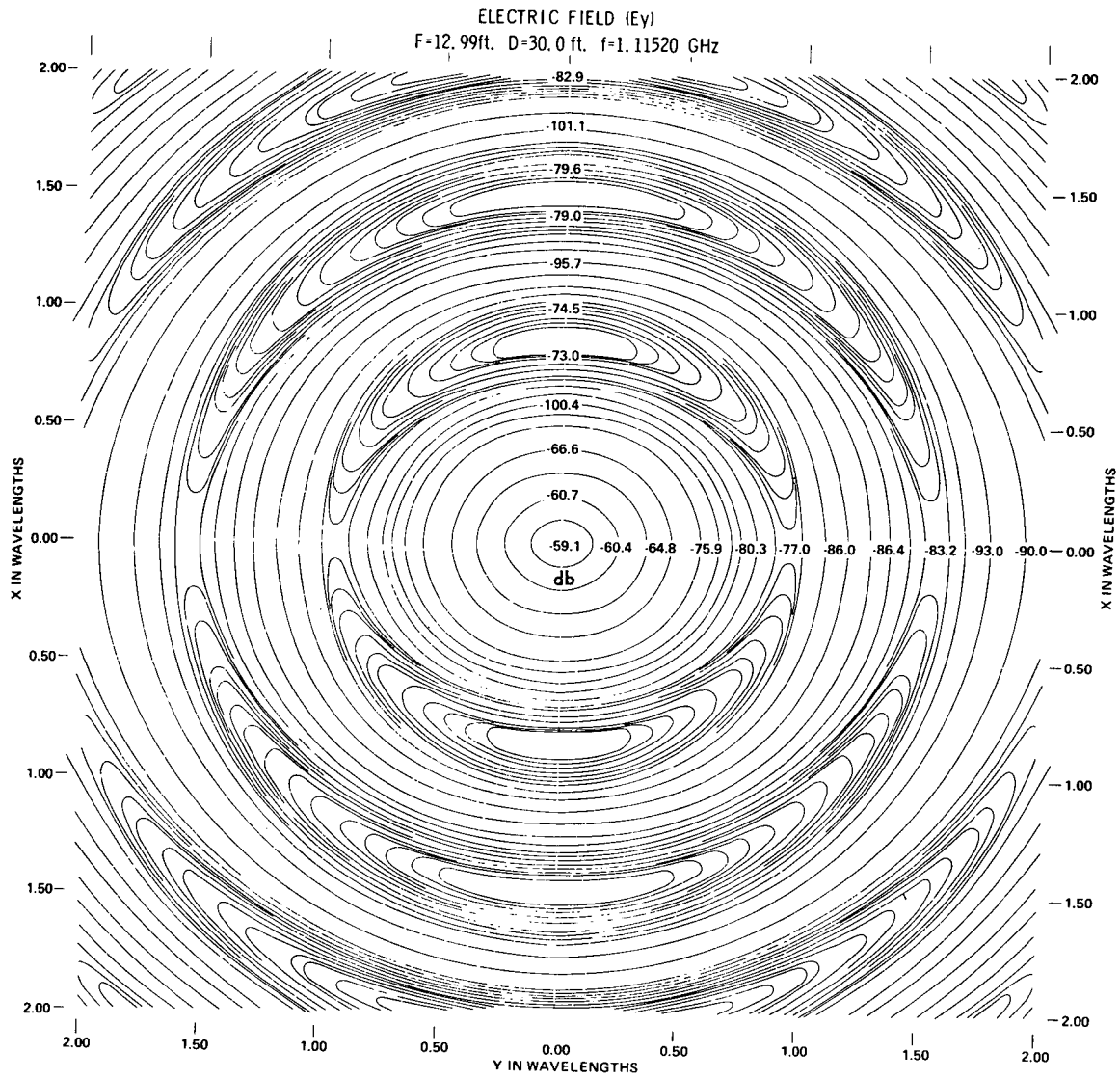

Figure 6. Airy disc and rings (axial reception)

F = 12.99 ft.
D = 30.0 ft.
f = 1.11520 GHz

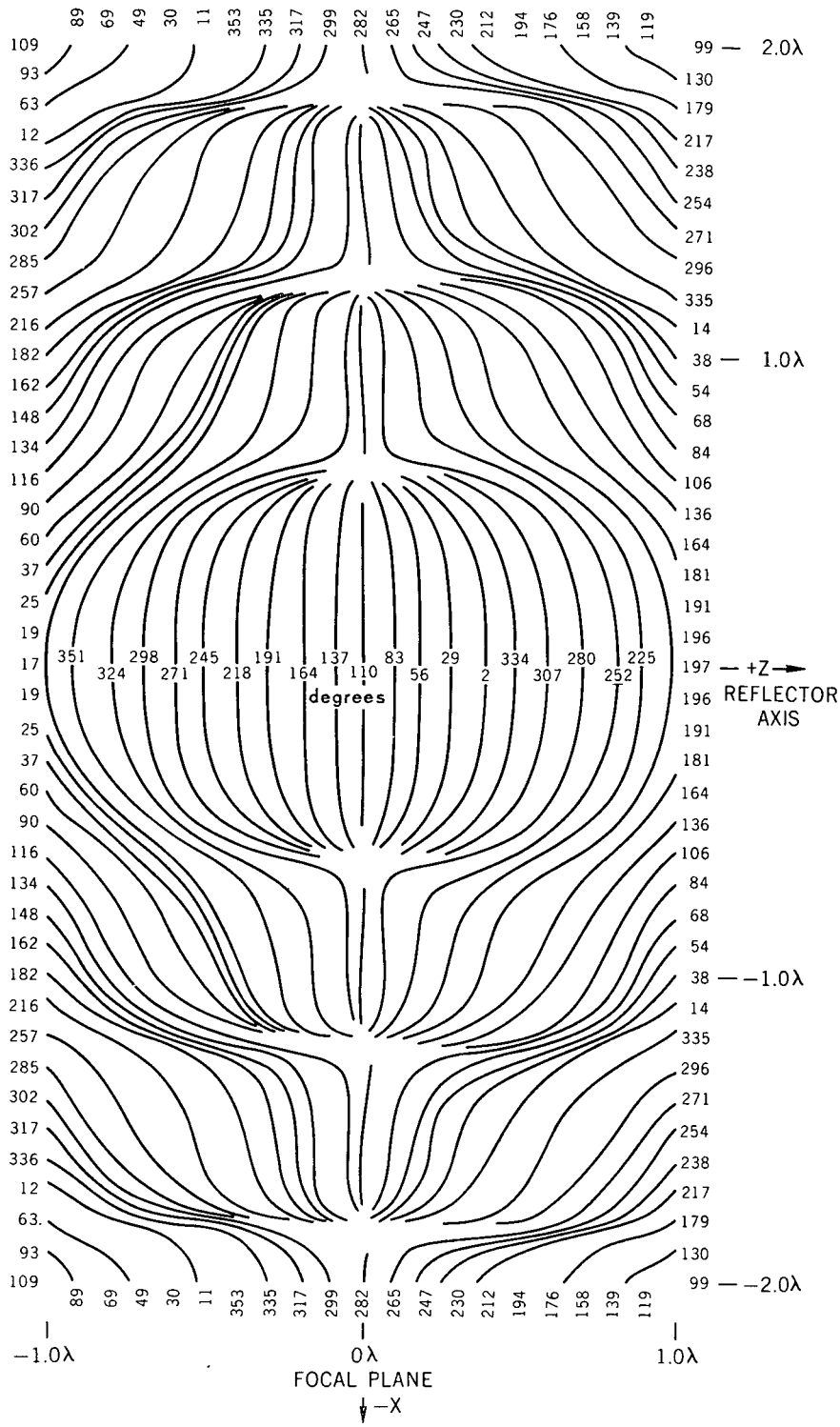

Figure 7. Phase of electric field near focal plane (axial reception)

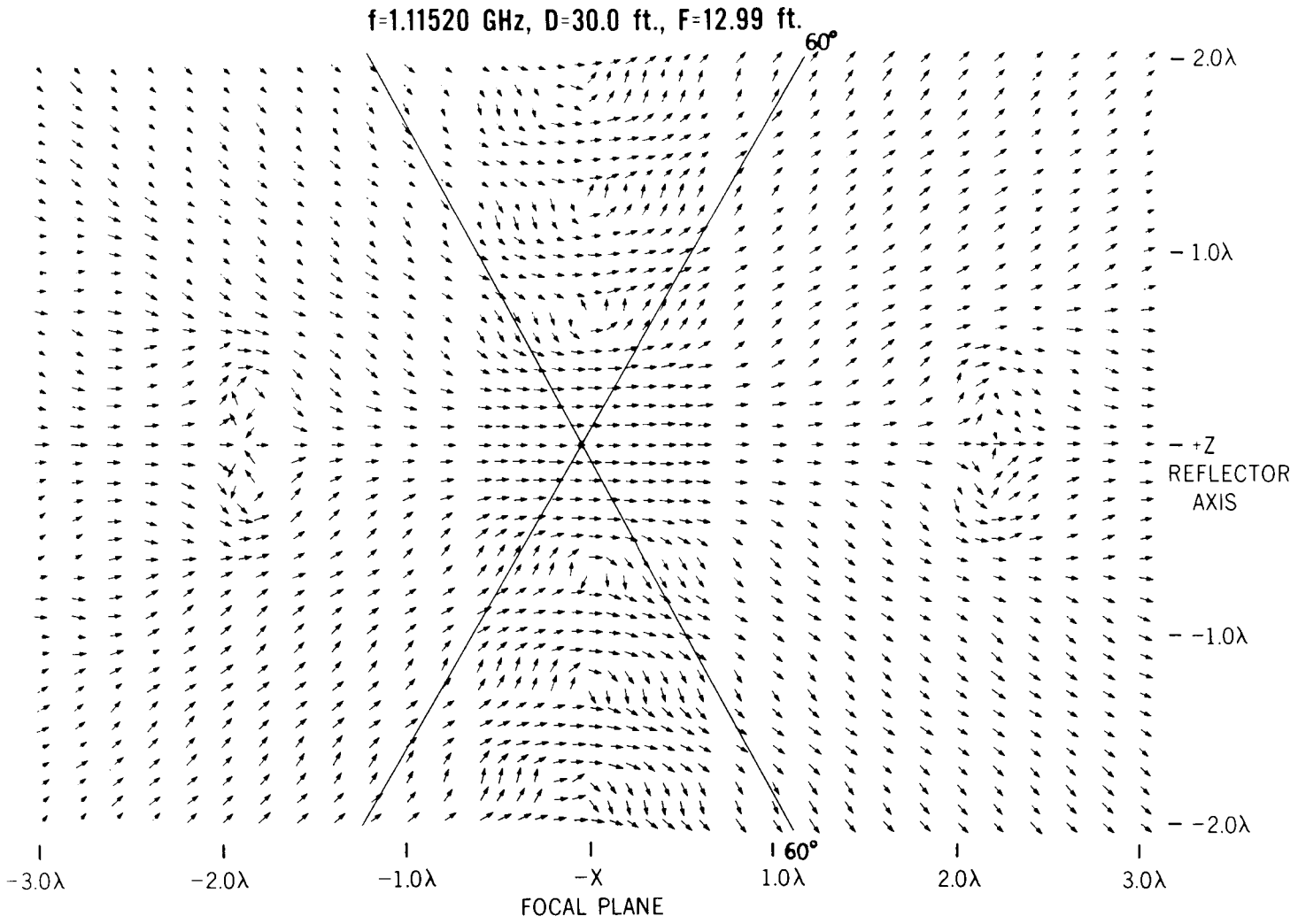

Figure 8. Direction of the time-average Pointing vector (axial reception)

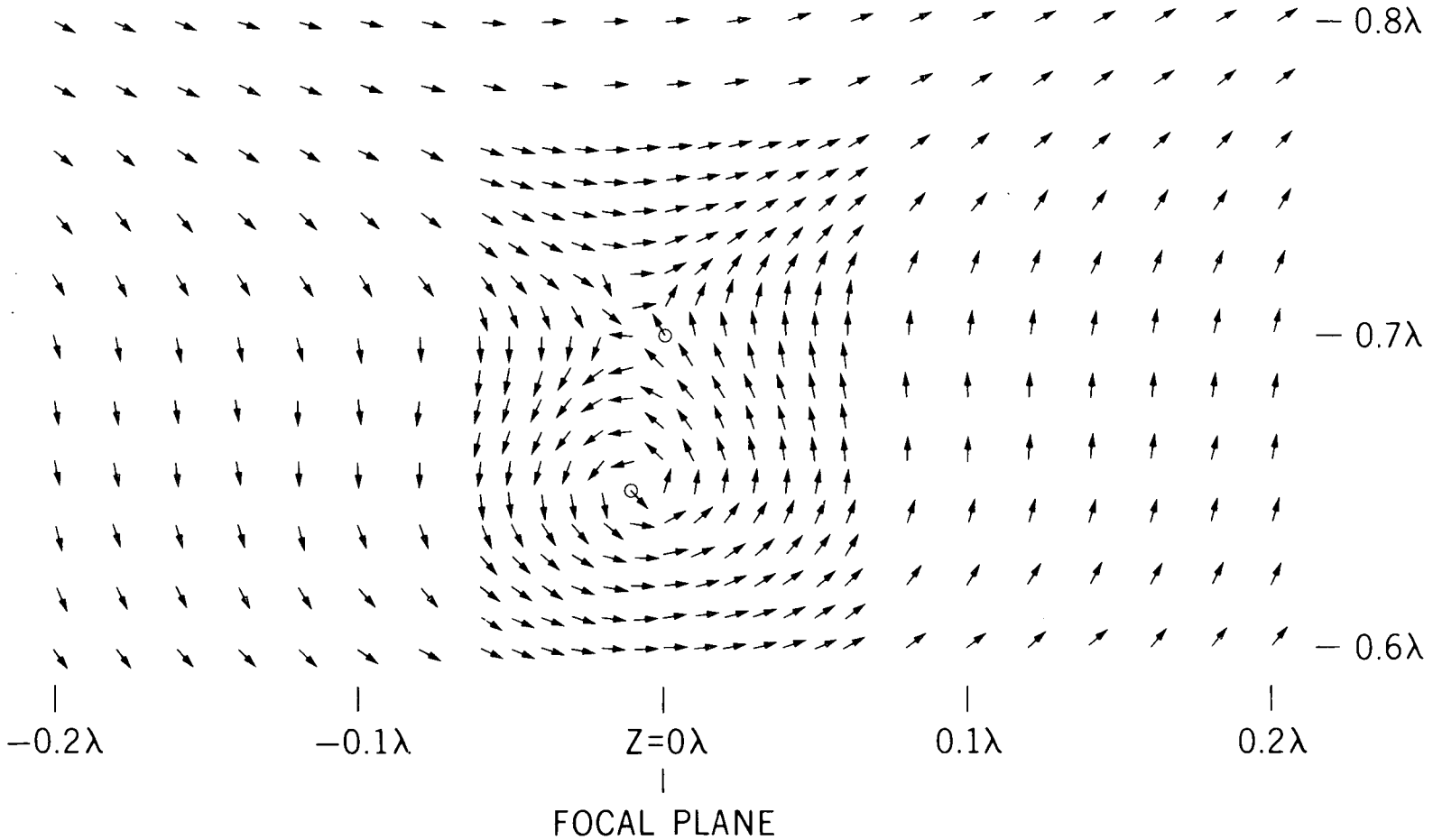

Figure 9. Direction of the time-average Pointing vector in the vicinity of a null (axial reception)

Additional information concerning the calculation and measurement of amplitude and phase in the image space (of a microwave lens) has been given by Farnell,[1], Bachynski, and Bekefi, [2]who applied scalar theory. Emphasis is placed on the fact that vector Kirchhoff-Kottler theory was used to obtain results presented in this document and that a numerical approach has been stressed to avoid many of the mathematical difficulties encountered in analysis, particularly for those cases where the diffracting system was complicated by intricate feeds, or illuminating sources, and non-conic or distorted surfaces. The latter are accommodated by the program without additional effort on the part of the program user, who simply modifies the input parameters, and the penalty in increased computer running-time (CPU time) is usually moderate.

A very simple illustration of the flexibility of the program is afforded by displacing the illuminating source so that a plane-wave (effectively) arrives with an arbitrary angle of inclination relative to the system axis (z-axis). The simulation produces this change for the source by calling Euler-angles in a rigid-body transformation and the components of a displacement vector. An inclination angle of 4-degrees was chosen, together with the same input parameters used previously for axial reception, based on the anticipated displacement of the intense field region associated with a focussing paraboloid. The equation

$$\sin \theta_s \cong \frac{K\Delta}{F}$$

relates beam squint-angle θ_s through beam-deviation factor K[3], feed displacement Δ, and focal length F. Under reciprocity then, for F/D = 0.433,

$$\sin 4^\circ \cong \frac{(.89)\ (\Delta)}{(12.99)}$$

and the energy can be expected to concentrate near

$$\Delta \approx 1.02 \text{ ft.} \Rightarrow 1.14\ \lambda\ @\ 1.11520 \text{ GHz},$$

on the opposite side of the z-axis.

---

[1] Ref. 16
Ref. 17
[2] Ref. 18
[3] Ref. 3, page 488

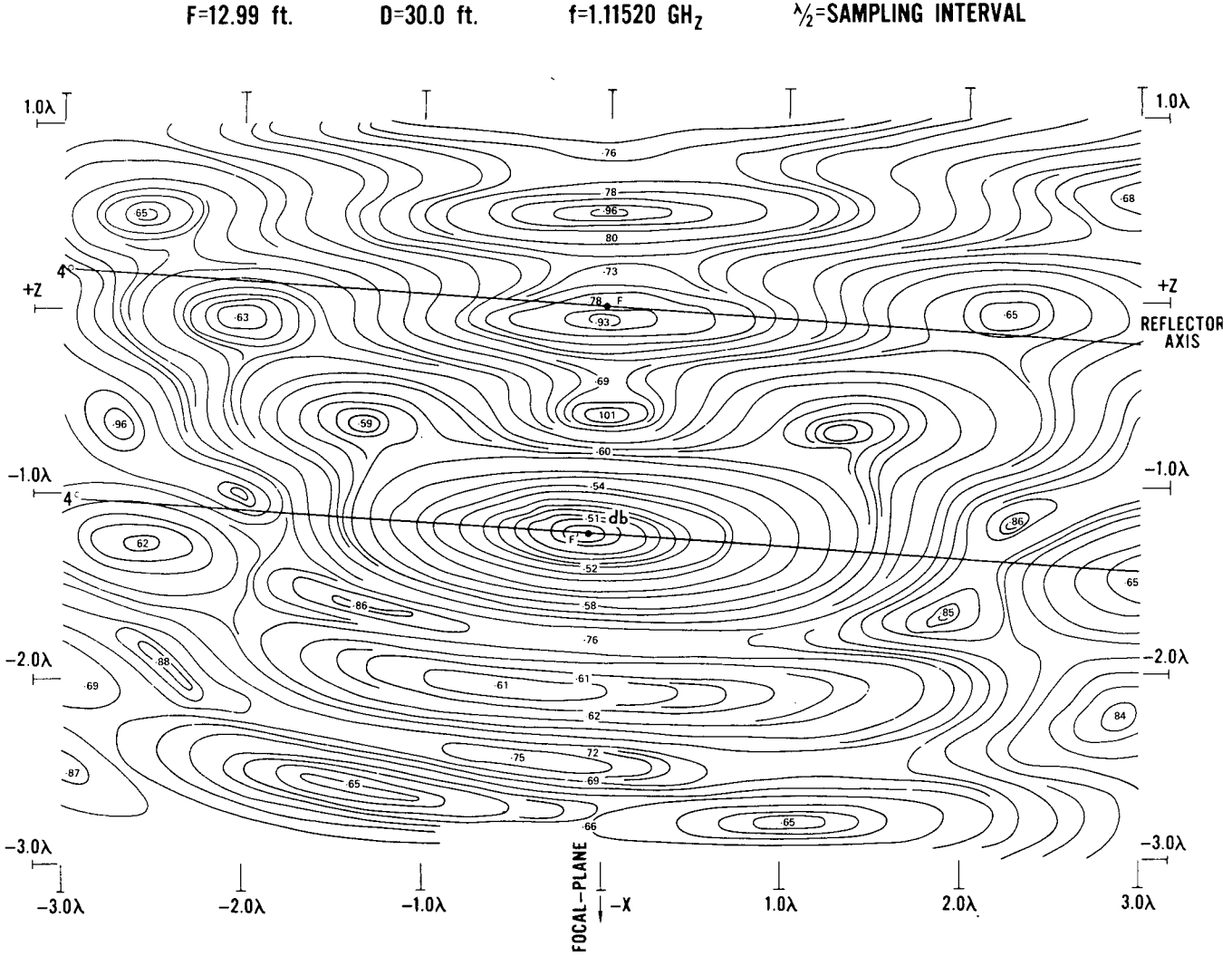

Figure 10. Amplitude of electric field near focal plane (paraxial reception)

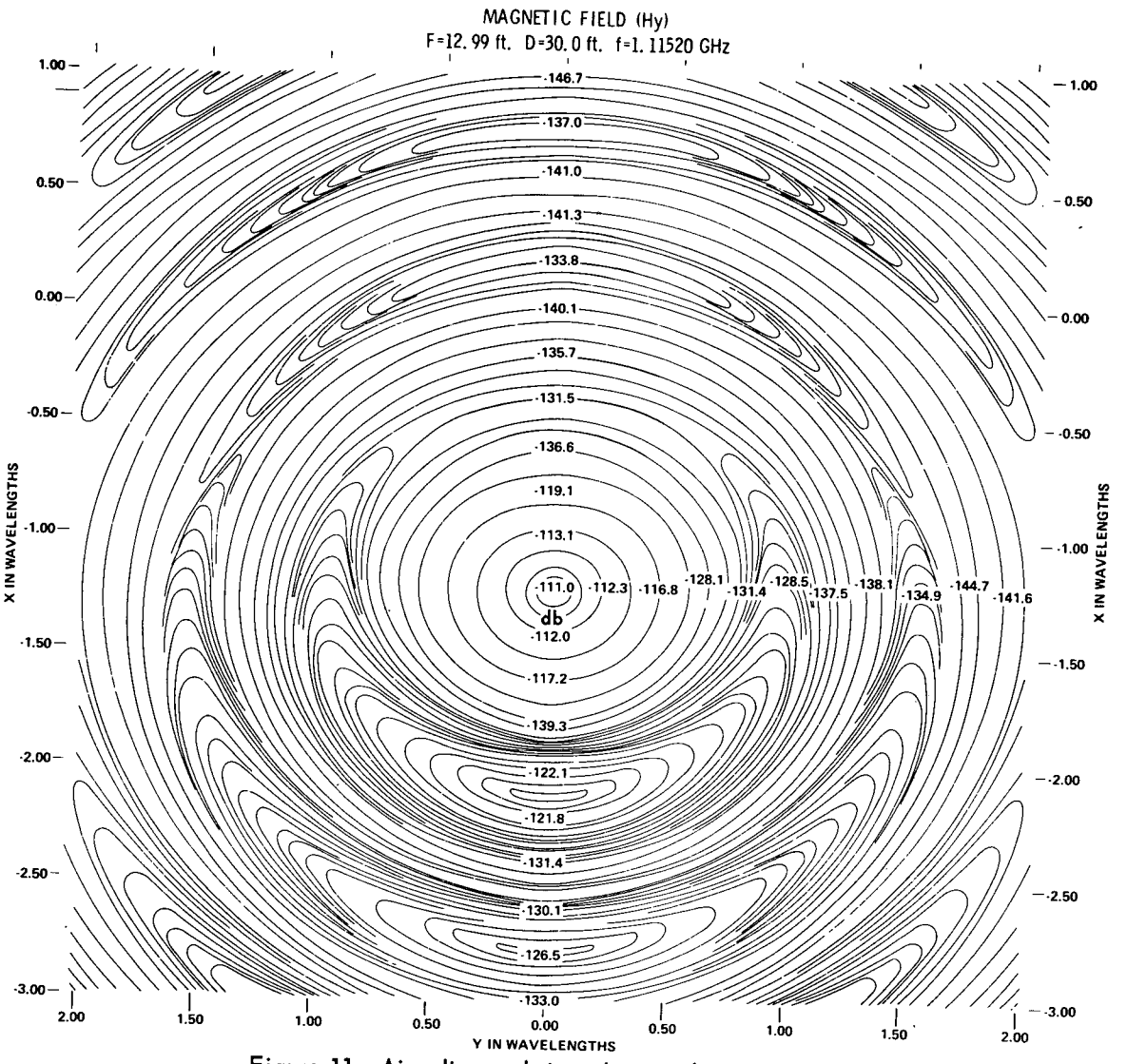

Figure 11. Airy disc and rings (paraxial reception)

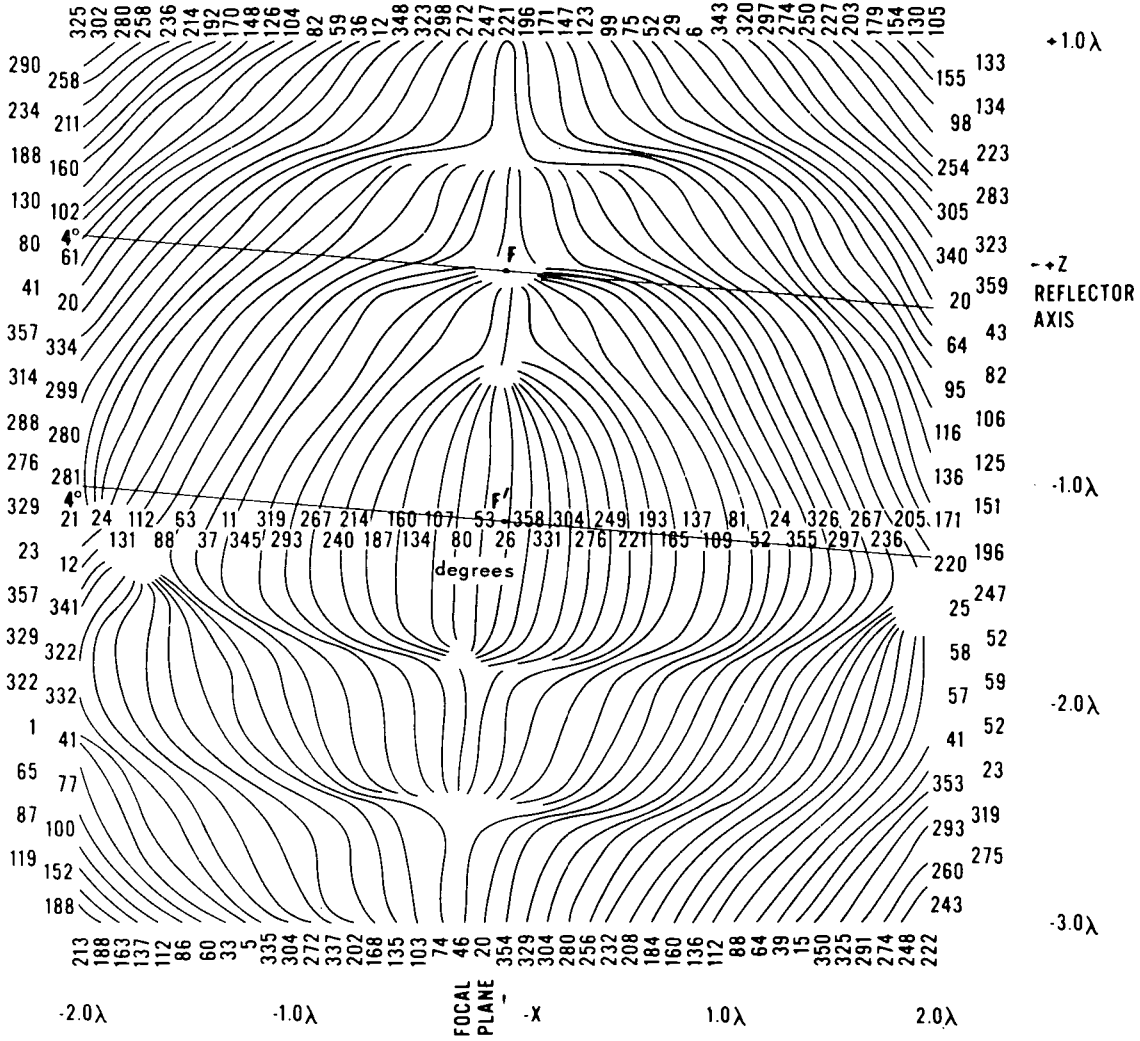

Figure 12. Phase of magnetic field near focal plane (paraxial reception)

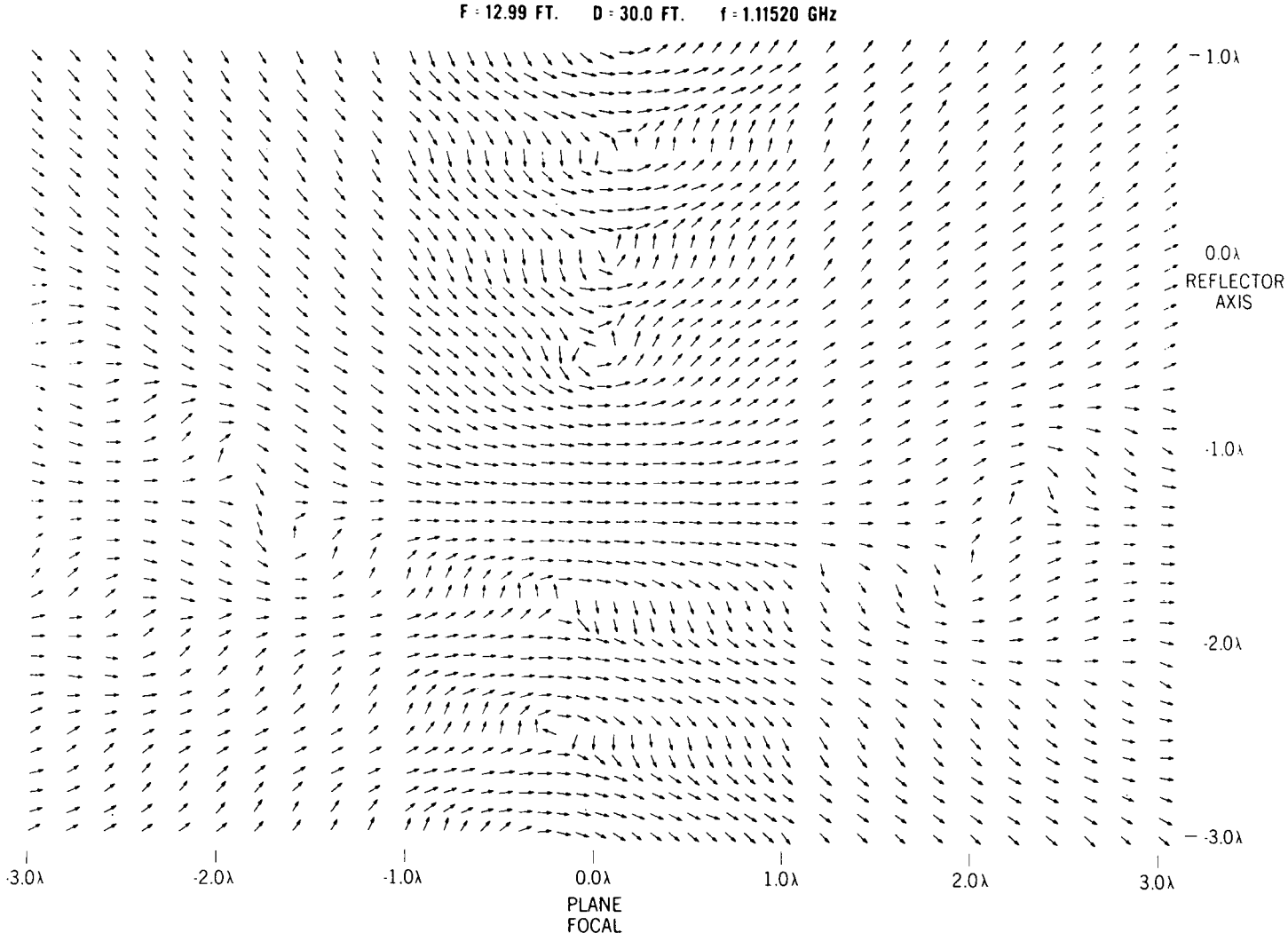

Figure 13. Direction of the time-average vector (paraxial reception)

A displaced and distorted version of the isophote field for axial reception is shown in Fig. 10. It appears that the peak intensity occurs just to the left of focal plane (toward the reflector). Solid lines at 4° are shown through F and F' as a reference for the displaced high intensity focal region. Fig. 11 shows the displaced Airy disc and rings in the x-y or focal plane. The wavefronts for the Fig. 10 computations are shown in Fig. 12. As before, the time-average Poynting vector was computed for the paraxial case. See Fig. 13. The Airy bright disc is displaced, together with the bright and dark rings. As with previous examples, power flow in the vicinity of dark rings and limits of the depth of field, which tends to be orthogonal to the general trend from left to right, is accompanied by large reductions in magnitude of the power density. The vectors $<\bar{P}>$ were not scaled at this writing because of the large amount of data reduction involved for this asymmetric example.

DUAL-REFLECTOR SYSTEMS

An initial effort to obtain the fields scattered from dual-reflector systems was undertaken by computing the Fraunhofer fields from a Cassegrain configuration. See Appendix C. Several idealizations were made, including omission of multiple reflections between γ_1 and γ_2, mutual coupling of the sheet currents, and even first-order blockage effects. The latter effects were taken into account previously in single-reflector systems by deleting the integration over the umbral region. A polygonal approximation to the shadow boundary was specified for each observer position.

The radiation pattern scattered by the main (parabolic) reflector was obtained as follows. A prime source $\mathfrak{I}_I = S_1 \cos^N \Theta$ was selected with N = 35.0 so that the feed taper plus space taper of the illumination at the edge of the (hyperbolic) subreflector equaled -9.0 db. The electric sheet current $\bar{K}_1$ on the hyperboloid γ_1 was then computed with contiguous increments of area not larger than 0.3λ by 0.3λ. Each value of sheet current $\bar{K}_2$ on the paraboloid γ_2 was then obtained by integrating over all of $\bar{K}_1$ on γ_1. A sampling grid not larger than 3.0λ by 3.0λ was used on the main reflector. Finally the distribution $\bar{K}_2$ was integrated in the Fraunhofer region for each observer position (r', θ', ϕ'). The distributions $\bar{K}_1$ and $\bar{K}_2$ are invariant with observer position and were therefore stored in the computer. For the reflector and feed geometries employed here, a four-fold symmetry exists for $\bar{K}_1$ and $\bar{K}_2$, however, this feature was not exploited even though cpu time can be conserved in such situations.

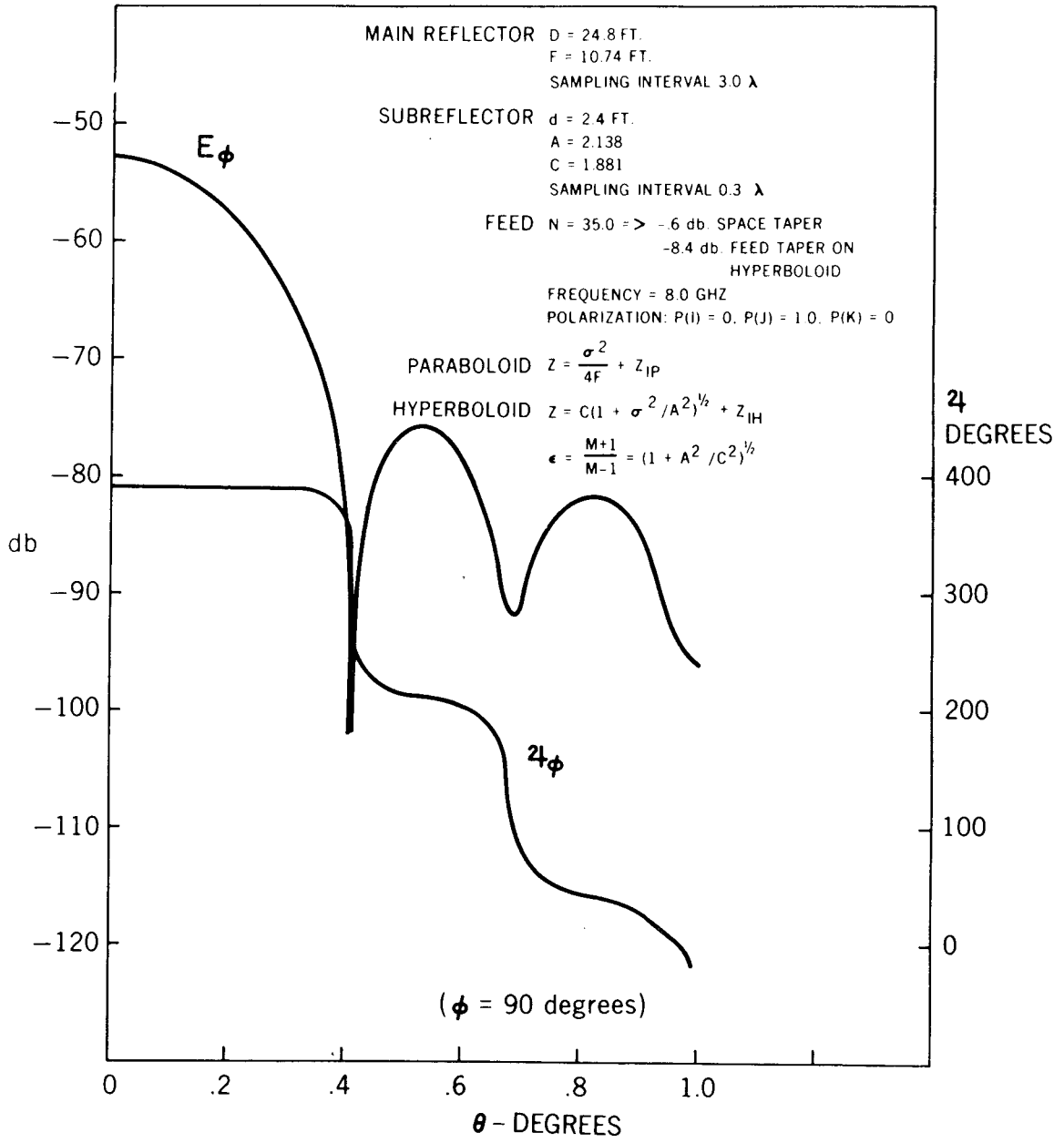

Figure 14. Dual-reflector system (cassegrain)

The results for the dual-reflector system, computed by applying Kirchhoff theory redundantly to the surfaces, are shown as Fig. 14. The degraded second-null is probably due to the sampling intervals chosen for integration of the distributions $\bar{K}_1$ and $\bar{K}_2$. The θ domain for Fig. 14 was adequately sampled ($\Delta\theta$ = 0.01 deg.) to detect the null, if it developed in the computations. This can be seen by an inspection of the phase characteristic ψ_θ which is also degraded in the vicinity of the second null. It is a more or less general rule that sampling intervals for sheet current distribution must be smaller for large values of θ.

The topics of sheet-current-distribution sampling and cpu time were also explored from the standpoint of stationary phase. For sufficiently high frequencies the geometric optics solution should be approached and, therefore, one might search for stationarity with the idea of reducing cpu time. The radial and azimuthal parameters, σ and ζ, used to generate the hyperboloid can be suitably restricted on γ_1 for a point on γ_2 at which $\bar{K}_2$ is to be evaluated. By this method only a portion of γ_1 is integrated – hopefully all of the stationary part, to the exclusion of the self-annihilating or non-stationary terms. The search for stationary phase regions was restricted by control over the radial variable (σ) alone in the initial attempt, but will be repeated with control over ζ, the angular variable, subsequently, to form increments of area. A typical increment of area on the hyperbolic subreflector will then be integrated by specifying σ_{min}, σ_{max}, ζ_{min}, ζ_{max}, and the observer point on γ_2 (for that region of $\bar{K}_1$ on γ_1) will be determined by geometrical optics. Preliminary results for one particular set of surface and feed parameters indicated that stationary contributions ranged over most of γ_2 when the observer position was in the vicinity of the vertex of γ_2. When the observer position was near the edge or limbs of γ_2, however, only an annular region of γ_1 appeared stationary.

A separate study of Cassegrain and Gregorian subsystems consisting of prime feed ($\mathfrak{F}'$) and subreflector (γ_1) was carried out to explore the geometrical optics conclusion that such a subsystem is effectively a virtual point source in the limit as $\lambda \to 0$. The feed $\mathfrak{F}_I$ is at the conjugate focus F* of γ_1 and the virtual source should appear at $\bar{F}$ of γ_1, which also coincides with F of γ_2 in the fully assembled system. Since the parameters used in the studies were not those of Fig. 14, graphical results are not presented here. For a hyperboloid diameter of 24λ and an ellipsoid diameter of 32λ it was found that the radius or range of observation relative to focus F could be reduced until, for wide angles, the distribution $\bar{K}_1$ or γ_1 was no longer optically visible. That is, the Cassegrain or Gregorian subsystems behaved as virtual point sources situated at F. Amplitude variations on a spherical locus of observation departed from a monotonic descent by about ±1 db typically. Phase variations on the same spherical locus of observation varied by approximately ±3 electrical degrees from the phase of a point source situated at F. In conclusion, as the

radius of observation is reduced ($R \rightarrow 0$) and the frequency is increased ($\lambda \rightarrow 0$) the observer does not lie in the near-zone ($2D^2/\lambda$) for the conics studied here since the scattering approximates that from a virtual source and D is effectively zero.

Preliminary calculations have been made for the "receive" mode of operation for dual reflectors, applying the theory of Appendix C with near-field integrals present. The Airy disc and rings have been observed in the conjugate focal plane for a coarse sampling (LI). A mapping of the focal region is planned for the example shown in Fig. 14, taking into account the domain of interest in the x-y and x-z planes for a magnification factor $M = (\epsilon + 1)/(\epsilon - 1)$. The optimum sampling ($LI_1$, LI_2) of the distributions $\bar{K}_1$ and $\bar{K}_2$ is not known at this time, and several computer runs will be required to establish a reasonable tradeoff between cpu time and accuracy of results. The magnified width of the Airy disc is a factor here since LI must usually be decreased as the observer moves off of the system axis. Over-sampling of $\bar{K}_1$ and $\bar{K}_2$ eventually establishes the "stability" of the solution with respect to LI, observer position, etc.

SUMMARY

The electric and magnetic fields, their associated phases, and the time-average Poynting vector were computed in the Fresnel and Fraunhofer regions for several well-known scatterers. Transmit and receive modes were discussed although, from a program standpoint, there is no logical distinction. A dual-reflector system was considered, and it appears that even multiple reflectors might be treated by the methods presented, however, the blockage (obscuration) problem requires additional effort.

Present plans call for extensive application of the existing program to ground-based and spacecraft antennas. Measured prime-feed data will be injected into the simulation and distorted antennas of various types will be treated. A variety of methods for obtaining directive gain and spillover will be compared and documented. Long-term plans include studies of multibeam polarization-diversity and frequency-diversity systems, shaped reflector and Schwarzschild configurations, parabolic cylinder antennas, spherical reflectors, and doubly curved surfaces. This document is an interim report.

ACKNOWLEDGMENTS

The author acknowledges input from the classical literature, periodicals, and journal papers. In addition, he has received help in the form of discussions and correspondence with numerous interested persons. Mr. Raymons Miezis of Programming Methods, Inc. provided most of the programming support over a period of several years and has succeeded in transforming the theory into a useful, working program. Mrs. Rose Kirkpatrick, of the same company, provided programming support and simplifications using assembly language. The author is also indebted to Mr. Anthony F. Durham, Branch Head, Antenna Systems Branch, Network Engineering Division, for helpful advice and discussions, and to Mr. Carl Riffe who assisted by developing a program for automatic plotting of the time-average Poynting vectors and made various suggestions, including alternative integration schemes on the current and charge distributions.

REFERENCES

1. Baker, B. B. and Copson, E. T., "The Mathematical Theory of Huygens' Principle," Oxford at the Clavendon Press, 1950, 1953

2. Stratton, J. A., "Electromagnetic Theory," McGraw-Hill Book Company, Inc., 1941

3. Silver, S. (ed.), "Microwave Antenna Theory and Design," McGraw-Hill Book Company, Inc., 1944

4. Born, M. and Wolf, E., "Principles of Optics," Pergamon Press, 1964

5. Skolnik, M., "Radar Handbook," McGraw-Hill Book Company, Inc., 1970

6. Sancer, M. I., "An Analysis of the Vector Kirchhoff Equations and the Associated Boundary-Line Charge," Radio Science, Vol. 3 (New Series), No. 2, 1968

7. Kaplan, W., "Advanced Calculus," Addison-Wesley Publishing Company, Inc., 1959

8. Schmidt, R. F., "The Calculation of Electromagnetic Fields by the Kirchhoff-Koffler Method," X-525-70-293, Goddard Space Flight Center, 1970

9. Rusch, W.V.T. and Potter, P. D., "Analysis of Reflector Antennas," Academic Press, 1970

10. Kraus, J. D., "Electromagnetics," McGraw-Hill Book Company, Inc. 1953

11. Gniss, vH., and Ries, G., "Feldbild um den Brennpunkt von Parabolreflektoren mit Kleinem F/D-Verhaltnis," Archiv der Elektrischen Übertragung (A.E.Ü.), Band 23, Oktober, 1969

12. Rudge, A. W., Davies, D.E.N., "Electronically Controllable Primary Feed for Profile-Error Compensation of Large Parabolic Reflectors," Proc. IEEE, Vol. 117, No. 2, February 1970

13. "The Microwave Engineer's Handbook and Buyer's Guide, Horizon House, 1965

14. Collin, R. E., and Zucker, F. J., "Antenna Theory," Part 2, McGraw-Hill Book Company, 1969

15. Minnett, H. C., and Thomas, B. Mac A., "Fields in the Image Space of Symmetrical Focussing Reflectors," Proc. IEE., Vol. 115, No. 10, October 1968

16. Farnell, G. W., "Calculated Intensity and Phase Distribution in the Image Space of a Microwave Lens," Canad. J. Phys., 1957, 35, pp. 777-783

17. Farnell, G. W., "Measured Phase Distribution in the Image Space of a Microwave Lens, Ibid, 1958, 36, pp. 935-943

18. Bachynski, M. P. and Bekefi, G., "Study of Optical Diffraction Images at Microwave Frequencies," J. Opt. Soc. Amer. 1957, 47, pp. 428-438

APPENDIX A

THE FORMULATION OF THE SCATTERED FIELDS $\overline{E}(x',y',z')$ $\overline{H}(x',y',z')$ BY EQUIVALENT METHODS

The following formulation of Stratton[1] was used, initially, to obtain fields, time-average Poynting vectors, isophotes and wavefronts

$$\overline{E}(x',\ y',\ z') = -\frac{1}{j\ \omega\ \epsilon}\ \frac{1}{4\pi} \oint_c \nabla\psi\ \overline{H}_1 \cdot d\overline{\ell} - \frac{1}{4\pi} \int_{S_1} [j\ \omega\mu\ (\overline{n} \times \overline{H}_1)\ \psi + (\overline{n} \cdot \overline{E}_1)\ \nabla\psi]\ ds$$

$$\overline{H}(x',\ y',\ z') = -\frac{1}{4\pi} \int_{S_1} (\overline{n} \times \overline{H}_1) \times \nabla\psi\ d\ s$$

$$\psi = \frac{e^{-jkr}}{r},\ \nabla\psi = -\left(j\ k + \frac{1}{r}\right)\psi\ \hat{1}_r.$$

An immediate conversion to the formulation used subsequently can be effected by making use of a relationship in one of Stratton's proofs.[2]

$$\int_{S_1} [(\overline{n} \times \overline{H}) \cdot \nabla)\ \nabla\psi\ d\ s = -\oint_c \nabla\psi\ \overline{H}_1 \cdot d\overline{\ell} - j\ \omega\ \epsilon \int_{S_1} (\overline{n} \cdot \overline{E})\ \nabla\psi\ d\ s$$

From the above, the equivalent form of the elctric field is

$$\overline{E}(x',\ y',\ z') = \frac{1}{j\ \omega\ \epsilon}\ \frac{1}{4\pi} \int_{S_1} [(\overline{n} \times \overline{H}) \cdot \nabla]\ \nabla\psi\ d\ s - j\ \omega\mu\ \frac{1}{4\pi} \int_{S_1} (\overline{n} \times \overline{H}_1)\ \psi\ d\ s.$$

The operator $\nabla_{\nabla\phi}$ of Stratton can be avoided by the use of dyadic notation.[3] It is noted that the equivalent form for the scattered electric field was obtained by Stratton in the course of demonstrating that the "historical" form of $E(x',y',z')$ satisfies Maxwell's equations.

[1] Ref. 2, page 469
[2] Ref. 2, page 470
[3] Ref. 8, pages 27-28

The equivalent form of the elctric field is also recognized in the general dyadic derivation of Sancer.[1] Attention is called to the fact that Sancer concludes with the forms of $\overline{E}(x',y',z')$ and $\overline{H}(x',y',z')$ of Stratton, and does not discuss the more compact formulation which disposes of the contour integral, the incident electric field $\overline{E}_i$, and its polarization vector $\overline{e}_i$.

In a recent text by Rusch and Potter,[2] the equivalent compact form for $\overline{E}(x',y',z')$ is presented together with a discussion of open surfaces. Sign variations appear between the formulations of Stratton, Sancer, Rusch and Potter, and Silver.[3] These appear to be due to conventions pertaining to the Green's function ψ and its gradient, $\nabla\psi$. In practice, for perfectly reflecting surfaces, the $\overline{E}(x',y',z')$ form has two integrals which must annihilate the radial fields and the $\overline{H}(x',y',z')$ form has only one integral. Signs, therefore, are not a vital issue here even though easy comparisons are occasionally frustrated by the appearance of what seems to be a spurious minus sign.

The text by Silver (1949) presents the "historical" form of $\overline{E}(x',y',z')$[4] and the compact equivalent form[5] as a specialization from volume to surface integration.[6] The "historical" form evolves when a single surface integral is equated to the sum of a surface-change integral plus a line-change integral. One might speculate on the consequences of a complete transformation of $E(x',y',z')$ to line-integral form[7] for open and closed surfaces.

[1] Ref. 6, page 142, equation (2.17)
[2] Ref. 9, page 46-47
[3] Ref. 3, page 160
[4] Ref. 3, page 160
[5] Ref. 3, page 132
[6] Ref. 3, page 87
[7] Ref. 1, page 79

APPENDIX B

THE TIME-AVERAGE POYNTING VECTOR

The time-average Poynting vector is defined[1, 2] as

$$\langle \bar{P} \rangle = \overline{\mathrm{Re}\,\bar{E}\,(x',\ y',\ z') \times \mathrm{Re}\,\bar{H}\,(\alpha',\ y',\ z')} = \frac{1}{2}\mathrm{Re}\,\bar{E}\,(x',\ y',\ z') \times \bar{H}^{*}\,(x',\ y',\ z')$$

It is noted that either the real part or the imaginary part of a complex solution (such as $\bar{E}$ or $\bar{H}$) may be chosen at the conclusion of a calculation to represent a physical state. For squares and products, however, the real part of the result is not equal to the product of the real parts, of $\bar{E}$ and $\bar{H}$, say. Details of the derivation of $< \bar{P} >$ can be found in several textbooks.[3]

The "working notation" of the digital computer program is the Cartesian vector basis, and the complex aspects of the solution are retained by separating real and imaginary components. After integration of the reflector surface the computer stores

$$E_{xR},\ E_{xI},\ E_{yR},\ E_{yI},\ E_{zR},\ E_{zI}$$

and

$$H_{xR},\ H_{xI},\ H_{yR},\ H_{yI},\ H_{zR},\ H_{zI},$$

the real and imaginary vector components of the electric and magnetic fields. Then the time-average Poynting vector

$$\langle \bar{P} \rangle = \frac{1}{2}\mathrm{Re}\,\bar{E}\,(x',\ y',\ z') \times \bar{H}^{*}\,(x',\ y',\ z')$$

$$= \frac{1}{2}\mathrm{Re}\,[\hat{i}\,(E_y H_z^{*} - E_z H_y^{*}) + \hat{j}\,(E_z H_x^{*} - E_x H_z^{*}) + \hat{k}\,(E_x H_y^{*} - E_y H_x^{*})]$$

$$= \frac{1}{2}\mathrm{Re}\,[\hat{i}\,\{(E_{yR} + j\,E_{yI})\,(H_{zR} - j\,H_{zI}) - (E_{zR} + j\,E_{zI})\,(H_{yR} - j\,H_{yI})\}$$

[1] Ref. 2, pp. 131-137
[2] Ref. 10, pp. 370-377
[3] Ref. 2, p. 136
Ref. 3, p. 70

$$+ \hat{j}\ \{\cdots\} + \hat{k}\ \{\cdots\}]$$

$$= \frac{1}{2}\,\mathrm{Re}$$

$$\hat{i}\ [(E_{yR}\,H_{zR} + E_{yI}\,H_{zI} - E_{zR}\,H_{yR} - E_{zI}\,H_{yI}) + j\ (E_{yI}\,H_{zR} - E_{yR}\,H_{zI}$$

$$- E_{zI}\,H_{yR} + E_{zR}\,H_{yI})] + \hat{j}\ [(\cdots) + j\ (\cdots)] + \hat{k}\ [(\cdots) + j\ (\cdots)]$$

$$= \frac{1}{2}\,[\hat{i}\ (E_{yR}\,H_{zR} + E_{yI}\,H_{zI} - E_{zR}\,H_{yR} - E_{zI}\,H_{yI})$$

$$+ \hat{j}\ (E_{zR}\,H_{xR} + E_{zI}\,H_{xI} - E_{xR}\,H_{zR} - E_{xI}\,H_{zI})$$

$$+ \hat{k}\ (E_{xR}\,H_{yR} + E_{xI}\,H_{yI} - E_{yR}\,H_{xR} - E_{yI}\,H_{xI})]$$

gives the time-average power flow in watts/meter^2.

APPENDIX C

FRAUNHOFER FIELDS FOR DUAL-REFLECTOR SYSTEMS[1]

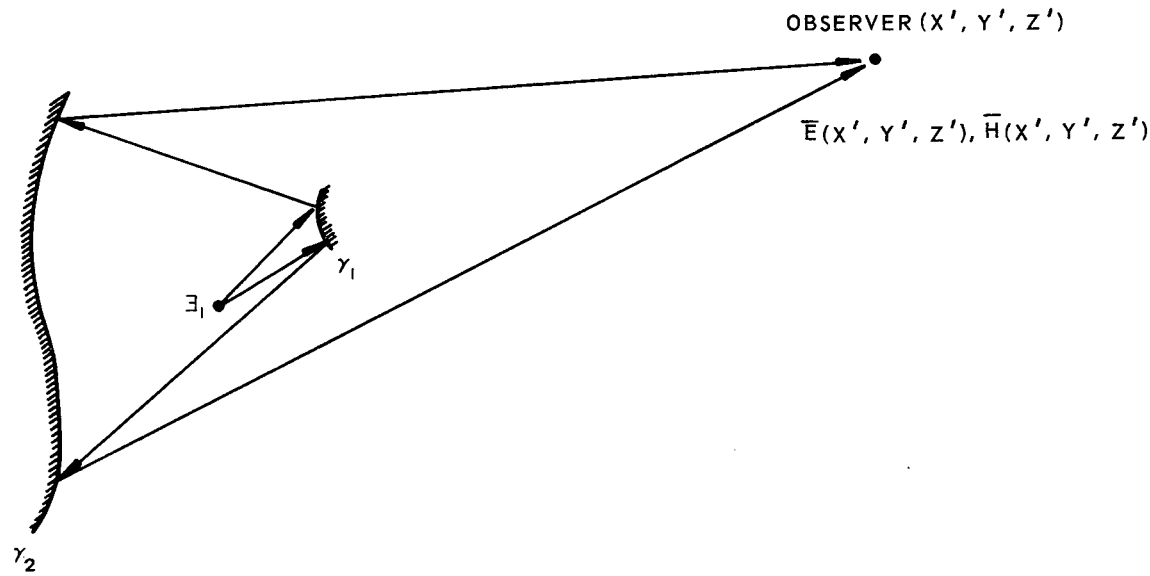

Figure C-1. Abstract Dual-reflector system

Consider a dual-reflector system as in Fig. C-1. The feed is designated $\Im_1$, main-reflector γ_2, and subreflector γ_1, Associated sheet currents, surface changes, line charges, and normals as given by $\bar{K}$, $\bar{q}_s$, $\bar{q}_\ell$, and n appropriately subscripted. The fields due to $\Im_1$ are proportional to $\bar{E}_1$, $\bar{H}_1$, the fields due to γ_1 are proportional to $\bar{E}_2$, $\bar{H}_2$, and the scattered fields due to γ_2 are designated $\bar{E}(x',y',z')$,.$\bar{H}(x',y',z')$.

[1] Due to Raymons Miezis of Computer Applications, Inc.

Assume initially that every point of γ_2 lies deep in the Fresnel region of γ_1, and that the observer is in the Fresnel region of γ_2. The general formulation is examined to determine what integrals must be evaluated.

$$\bar{E}(x', y', z') = \frac{1}{j\omega\epsilon}\frac{1}{4\pi}\int_{S_2}[(\bar{n}_2 \times \bar{H}_2)\cdot\nabla]\nabla\psi - j\omega\mu\frac{1}{4\pi}\int_{S_2}(\bar{n}_2 \times \bar{H}_2)\psi\, ds$$

$$\bar{H}(x', y', z') = -\frac{1}{4\pi}\int_{S_2}(\bar{n}_2 \times \bar{H}_2)\times\nabla\psi\, ds.$$

Now only $\bar{H}_2$ is required above, and

$$\bar{H}_2(x_2, y_2, z_2) = -\frac{1}{4\pi}\int_{S_1}(\bar{n}_1 \times \bar{H}_1)\times\nabla\psi\, ds.$$

Since the observer is assumed to be in the Fraunhofer region of γ_2 here, the transverse fields are obtained from

$$\bar{E}(\infty, \theta', \phi') = -j\omega\mu\frac{1}{4\pi}\int_{S_2}(\bar{n}_2 \times \bar{H}_2)\psi\, ds$$

projected onto the basis vectors $\hat{1}_{\theta'}$ and $\hat{1}_{\phi'}$. $\bar{H}(\infty, \theta', \phi')$ is most economically obtained from the auxiliary relationship

$$\frac{|\bar{E}(\infty, \theta', \phi')|}{|\bar{H}(\infty, \theta', \phi')|} = z_0$$

In this formulation only $\bar{H}_2$ is required and only two integrals, $\bar{H}_2(x_2, y_2, z_2)$ and $\bar{E}(\infty, \theta', \phi')$ are evaluated since the observer is in the Fraunhofer region, compared with four integrals for the general case, observer in the Fresnel zone.

The advantages of the compact equivalent form of the electric field can now be seen. If E(x',y',z') were written in the "historical" form

$$\bar{E}(x', y', z') = -\frac{1}{j\omega\epsilon}\frac{1}{4\pi}\int_{c_2}\nabla\psi\,\bar{H}_2\cdot d\bar{\ell} - \frac{1}{4\pi}\int_{S_2}[(j\omega\mu(\bar{n}_2\times\bar{H}_2)\psi + \bar{n}_2\cdot\bar{E}_2)\nabla\psi]\, ds$$

for the Fresnel region of γ_2, $\bar{E}_2$ as well as $\bar{H}_2$ would be required for the evaluation. But

$$\bar{E}_2(x_2, y_2, z_2) = -\frac{1}{j\omega\epsilon}\frac{1}{4\pi}\int_{c_1}\nabla\psi\bar{H}_1\cdot d\bar{\ell}_1 - \frac{1}{4\pi}\int_{S_1}[j\omega\mu(\bar{n}_1\times\bar{H}_1)\psi + (\bar{n}_1\cdot\bar{E}_1)\nabla\psi]\,ds,$$

which is complicated by the appearance of a contour integral and involves a mixture of electric and magnetic fields in the integrands.